Simplified Viscous/Inviscid Analysis for Nearly-Axisymmetric Bodies

Mark Drela 14 Sep 16

1 Summary

The method described here uses a compressible extension of the old Von Karman airship method [1] to describe the potential flow, and an axisymmetric version of the integral boundary layer formulation of XFOIL [2] to describe the surface boundary layer and trailing wake. The two formulations are strongly coupled and solved simultaneously using the XFOIL methodology. Effects such as flow separation can thus be captured. The intent of this strongly-coupled viscous/inviscid method is to obtain reasonable drag prediction accuracy together with extreme computational speed.

2 Geometry

The body geometry is described by the area $A_{(x)}$ and perimeter $b_{0(x)}$ distributions, as shown in Figure 1, with x being the axial coordinate. For a body of circular cross-section these are related by

$$4\pi A \;=\; b_0^2 \qquad\qquad \text{(round body)} \tag{1}$$

but considering them to be independent allows reasonably accurate drag calculation of bodies which are slender but not axisymmetric.

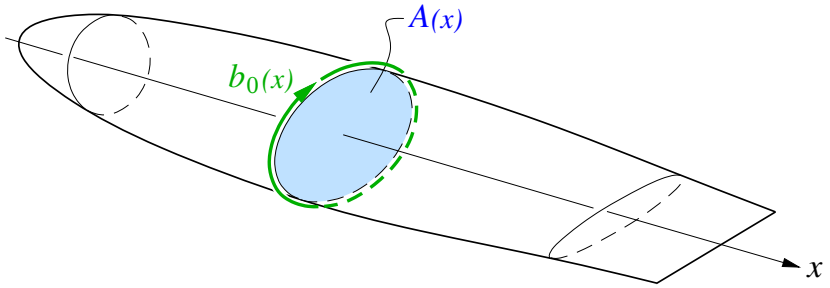

Figure 1: Slender body with cross-sectional area $A_{(x)}$ and perimeter $b_{0(x)}$.

3 Potential Flow Calculation

To compute the potential flow, an equivalent axisymmetric body of radius $R_{(x)}$ is first defined.

$$R_{(x)} \;=\; \sqrt{\frac{A_{(x)}}{\pi}} \tag{2}$$

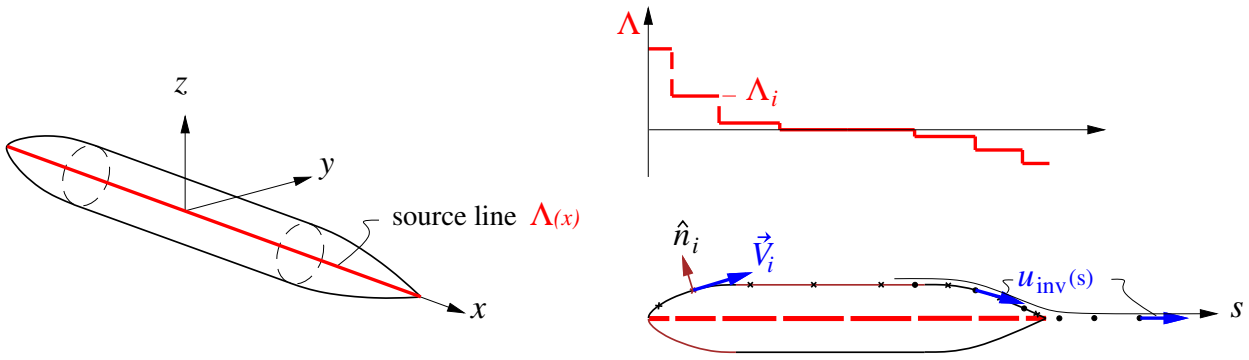

Figure 2: Fuselage potential flow model using compressible source line on axis.

The compressible potential flow about this body is represented with piecewise-constant line sources placed on the axis, as sketched in Figure 2.

The cartesian perturbation velocities of $i = 1, 2 \ldots n$ such segments located between points $x_1, x_2, \ldots x_{N+1}$ are

$$u(x,y,z) = \sum_{i=1}^{N} \frac{\Lambda_i}{4\pi\,\beta^2} \left(\frac{1}{r_{i+1}} - \frac{1}{r_i} \right) \tag{3}$$

$$v(x,y,z) = \sum_{i=1}^{N} \frac{\Lambda_i}{4\pi\,\beta} \left(\frac{x_{i+1}-x}{r_{i+1}} - \frac{x_i-x}{r_i} \right) \frac{\beta y}{(\beta y)^2 + (\beta z)^2} \tag{4}$$

$$w(x,y,z) = \sum_{i=1}^{N} \frac{\Lambda_i}{4\pi\,\beta} \left(\frac{x_{i+1}-x}{r_{i+1}} - \frac{x_i-x}{r_i} \right) \frac{\beta z}{(\beta y)^2 + (\beta z)^2} \tag{5}$$

$$\text{where} \qquad \beta^2 \equiv 1 - M_\infty^2 \tag{6}$$

$$r_i(x,y,z) \equiv \sqrt{(x-x_i)^2 + (\beta y)^2 + (\beta z)^2} \tag{7}$$

$$r_{i+1}(x,y,z) \equiv \sqrt{(x-x_{i+1})^2 + (\beta y)^2 + (\beta z)^2} \tag{8}$$

Setting flow tangency at each of the N control points on the actual body surface with normal vectors $\hat{\mathbf{n}}_i$

$$[(V_\infty + u_i)\,\hat{\mathbf{x}} + v_i\,\hat{\mathbf{y}} + w_i\,\hat{\mathbf{z}}] \cdot \hat{\mathbf{n}}_i = 0 \tag{9}$$

gives a $N \times N$ linear system for the source strengths Λ_i. Because the control points are not immediately adjacent to the source elements, this system becomes increasingly ill-conditioned as N is increased, especially with non-slender bodies. However, with the cosine spacing sketched in Figure 2, essentially converged results are obtained for $N = 25$ or less, with very great computational economy.

A proper axisymmetric panel method is of course an alternative to the present approach, but would greatly increase the code complexity, and also the system setup time which would dominate the system solution time for these small number of unknowns. These additional drawbacks favor the simple present approach.

4 Viscous Flow Calculation

4.1 Axisymmetric boundary layer and wake equations

All viscous calculations are performed in the meridional arc length coordinate s, defined from the equivalent $R_{(x)}$ distribution.

$$s_{(x)} \;=\; \int^{x} \sqrt{1+(\mathrm{d}R/\mathrm{d}x)^2}\;\mathrm{d}x \tag{10}$$

This is continued into the wake where $R=0$ is specified.

The axisymmetric momentum and kinetic energy boundary layer equations governing the viscous boundary layers and wake are as follows.

$$\frac{\mathrm{d}\left(\rho_e u_e^2 \Theta\right)}{\mathrm{d}s} \;=\; b\,\frac{\tau_w}{2} \;-\; \rho_e u_e \Delta^* \frac{\mathrm{d}u_e}{\mathrm{d}s} \tag{11}$$

$$\frac{\mathrm{d}\left(\frac{1}{2}\rho_e u_e^3 \Theta^*\right)}{\mathrm{d}s} \;=\; (b\mathcal{D}) \;-\; \rho_e u_e^2 \Delta^{**} \frac{\mathrm{d}u_e}{\mathrm{d}s} \tag{12}$$

Here, b is an effective perimeter shown in Figure 3 which arises when the various areas Δ^*, Θ etc. in the equations above are approximated with their 2D equivalents.

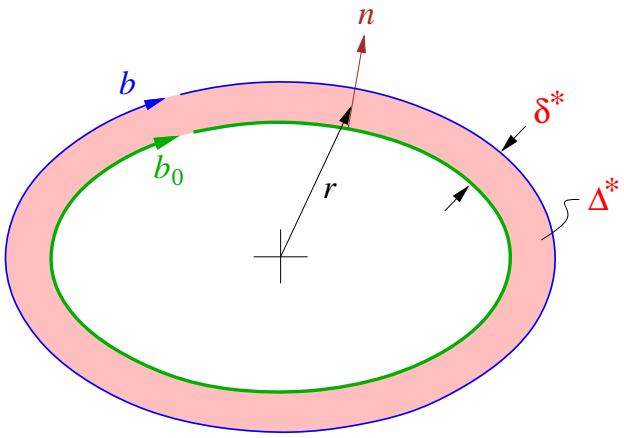

Figure 3: Body perimeter b_0, displacement area Δ^*, and effective perimeter b.

For example, the definition of the displacement area is

$$\Delta^* \;=\; \int_0^{n_e} \left(1-\frac{\rho u}{\rho_e u_e}\right) 2\pi r\;\mathrm{d}n \tag{13}$$

which has the somewhat awkward radius r inside the integral. This is suitably approximated by its average value over the layer thickness, by using the 2D displacement thickness itself,

$$2\pi r \;\simeq\; b_0 \,+\, 2\pi\delta^* \;\equiv\; b \tag{14}$$

so that the modified perimeter b is taken as a suitable approximate value for the local perimeter $2\pi r_{(n)}$ over the integral. This allows all the viscous areas to be expressed in terms

of the more familiar 2D integral thicknesses as follows.

$$\delta^* = \int_0^{n_e} \left(1 - \frac{\rho u}{\rho_e u_e}\right) \mathrm{d}n \tag{15}$$

$$\theta = \int_0^{n_e} \left(1 - \frac{u}{u_e}\right) \frac{\rho u}{\rho_e u_e} \, \mathrm{d}n \tag{16}$$

$$\theta^* = \int_0^{n_e} \left(1 - \frac{u^2}{u_e^2}\right) \frac{\rho u}{\rho_e u_e} \, \mathrm{d}n \tag{17}$$

$$\delta^{**} = \int_0^{n_e} \left(1 - \frac{u^2}{u_e^2}\right) \frac{\rho u}{\rho_e u_e} \, \mathrm{d}n \tag{18}$$

$$\Delta^* = \int_0^{n_e} \left(1 - \frac{\rho u}{\rho_e u_e}\right) 2\pi r \, \mathrm{d}n \simeq b\,\delta^* \tag{19}$$

$$\Theta = \int_0^{n_e} \left(1 - \frac{u}{u_e}\right) \frac{\rho u}{\rho_e u_e} \, 2\pi r \, \mathrm{d}n \simeq b\,\theta \tag{20}$$

$$\Theta^* = \int_0^{n_e} \left(1 - \frac{u^2}{u_e^2}\right) \frac{\rho u}{\rho_e u_e} \, 2\pi r \, \mathrm{d}n \simeq b\,\theta^* \tag{21}$$

$$\Delta^{**} = \int_0^{n_e} \left(1 - \frac{\rho}{\rho_e}\right) \frac{u}{u_e} \, 2\pi r \, \mathrm{d}n \simeq b\,\delta^{**} \tag{22}$$

The dissipation integral is also defined in terms of its 2D form.

$$\mathcal{D} = \int_0^{n_e} \tau \frac{\partial u}{\partial n} \, \mathrm{d}n \tag{23}$$

$$(b\mathcal{D}) = \int_0^{n_e} \tau \frac{\partial u}{\partial n} \, 2\pi r \, \mathrm{d}n \simeq b\,\mathcal{D} \tag{24}$$

Using the approximate area definitions above, equations (11) and (12) are put in their equivalent logarithmic differential forms.

$$\mathrm{d}\,\ln\theta + \mathrm{d}\,\ln b = \frac{s}{\theta}\frac{c_f}{2}\,\mathrm{d}\,\ln s - \left(H + 2 - M_e^2\right)\,\mathrm{d}\,\ln u_e \tag{25}$$

$$\mathrm{d}\,\ln H^* = \left(\frac{s}{\theta}\frac{2c_{\mathcal{D}}}{H^*} - \frac{s}{\theta}\frac{c_f}{2}\right)\mathrm{d}\,\ln s - \left(\frac{2H^{**}}{H^*} + 1 - H\right)\mathrm{d}\,\ln u_e \tag{26}$$

Equation (26) is actually the difference between the logarithmic forms of equations (12) and (11). The usual 2D shape parameter is defined as

$$H = \frac{\delta^*}{\theta} \tag{27}$$

and the 2D integral relations

$$\frac{\tau_w}{\frac{1}{2}\rho_e u_e^2} = c_f(H, Re_\theta, M_e^2) \tag{28}$$

$$\frac{\mathcal{D}}{\rho_e u_e^3} = c_{\mathcal{D}}(H, Re_\theta, M_e^2) \tag{29}$$

$$\frac{\theta^*}{\theta} = H^*(H, Re_\theta, M_e^2) \tag{30}$$

$$\frac{\delta^{**}}{\theta} = H^{**}(H, Re_\theta, M_e^2) \tag{31}$$

are used to close the equations. Except for the trivial additional term $d \ln b$ in (25), all these relations are identical to their 2D forms, so that an existing 2D implementation can be used with only minimal modification.

4.2 Direct BL solution

In the classical BL formulation, $u_{e(s)}$ is prescribed to be the inviscid velocity, e.g.

$$u_e \;=\; u_{\rm inv} \tag{32}$$

This can be obtained from the Λ_i strengths computed above, by using them in the u, v, w summations (3,4,5) to compute the inviscid surface tangential velocities $u_{{\rm inv}(s)}$ along the surface and also into the wake.

$$u_{{\rm inv}(s)} \;=\; \sqrt{u^2 + v^2 + w^2} \tag{33}$$

Once $u_{e(s)}$ is specified, then equations (25) and (26) can in principle be solved for the boundary layer variables $\theta_{(s)}, \delta^*_{(s)}$ by usual downstream ODE integration. However, if separation is encountered this integration will fail. The reason is that ${\rm d}H^*/{\rm d}H \simeq 0$ at separation, for which equation (26) will then produce ${\rm d}\delta^*/{\rm d}s \to \infty$ so the downstream integration cannot proceed. This is the usual Goldstein separation singularity.

4.3 Viscous/Inviscid interacted solution

The present method eliminates the separation singularity by the usual viscous/inviscid interaction formulation. Using the wall-blowing concept, the actual viscous edge velocities $u_{e(s)}$ seen by the boundary layer and wake are modified by adding contributions from the apparent wall-blowing sources, assumed to be axisymmetric point sources at the $j \ldots j+1$ interval midpoints.

$$u_{e_i} \;=\; u_{{\rm inv}_i} \;+\; \frac{1}{\rho_{e_i}} \sum_j \frac{1}{4\pi} \frac{m_{j+1} - m_j}{\left| s_i - \frac{1}{2}(s_{j+1}+s_j) \right| \left(s_i - \frac{1}{2}(s_{j+1}+s_j) \right)} \tag{34}$$

Here, m is the axisymmetric mass defect, defined by

$$m \;=\; \rho_e u_e \Delta^* \;=\; \int_0^{n_e} (\rho_e u_e - \rho u)\, 2\pi r \, {\rm d}n \;\simeq\; \rho_e u_e \delta^* (b_0 + 2\pi\delta^*) \tag{35}$$

which is a quadratic equation giving δ^* in terms of m and u_e.

$$\delta^* \;=\; \frac{1}{4\pi} \left(-b_0 + \sqrt{b_0^2 + \frac{8\pi\, m}{\rho_e u_e}} \right) \tag{36}$$

The summation (34) can be put into a more concise form by precomputation of the mass-influence matrix d_{ij} which depends only on the geometry.

$$u_{e_i} \;=\; u_{{\rm inv}_i} \;+\; \frac{1}{\rho_{e_i}} \sum_j d_{ij}\, m_j \tag{37}$$

$$d_{ij} \;=\; \frac{1}{4\pi} \left[\frac{1}{\left| s_i - \frac{1}{2}(s_j+s_{j-1}) \right| \left(s_i - \frac{1}{2}(s_j+s_{j-1}) \right)} - \frac{1}{\left| s_i - \frac{1}{2}(s_{j+1}+s_j) \right| \left(s_i - \frac{1}{2}(s_{j+1}+s_j) \right)} \right] \tag{38}$$

In the viscous/inviscid solution scheme, the boundary layer equations (25) and (26) are solved together with the u_e definition equation (37), to obtain the overall solution $\theta_{(s)}$, $\delta^*_{(s)}$, $u_{e(s)}$. Only the inviscid velocity $u_{\mathrm{inv}(s)}$ is prescribed. Because equation (37) has global influence, the equations are not solved by marching, but instead are solved "everywhere" at once by a global Newton iteration, thus avoiding the Goldstein singularity. An initial marching calculation with $u_e = u_{\mathrm{inv}}$ prescribed (and necessarily modified at separation) is still used to obtain a good initial guess to start the Newton cycle.

4.4 Drag and dissipation calculation

In the absence of any boundary layer ingestion, the body profile drag is the far-downstream momentum defect. This is extrapolated from the boundary layer values at the numerical end of the wake, denoted by $(\,)_{\mathrm{end}}$.

$$H_\infty = 1 + (\gamma - 1) M_\infty^2 \tag{39}$$

$$H_{\mathrm{end}} = \frac{\Delta^*_{\mathrm{end}}}{\Theta_{\mathrm{end}}} \tag{40}$$

$$H_{\mathrm{avg}} = \tfrac{1}{2}\left(H_{\mathrm{end}} + H_\infty\right) \tag{41}$$

$$D = \rho_\infty V_\infty^2 \Theta_\infty = (\rho_e u_e^2 \Theta)_{\mathrm{end}} \left(\frac{(u_e)_{\mathrm{end}}}{V_\infty} \right)^{H_{\mathrm{avg}}} \tag{42}$$

$$C_D \equiv \frac{D}{\frac{1}{2}\rho_\infty V_\infty^2 S_{\mathrm{ref}}} = \frac{2\Theta_\infty}{S_{\mathrm{ref}}} \tag{43}$$

Expression (39) assumes the body is adiabatic so that the mass-averaged total enthalpy in the wake has the freestream value.

Equation (42) is the integrated momentum equation (11) with the assumption that $H_{(s)}$ varies linearly with $\ln u_{e(s)}$, which is generally accurate in the far wake. It is also equivalent to the Squire-Young profile drag formula, extended to the compressible case. By comparing the Θ and Θ^* definitions (20) and (21) far downstream where $u_{(n)} \to V_\infty$, we also have the following useful relation for the far-downstream kinetic energy area.

$$\Theta^*_\infty = 2\Theta_\infty \tag{44}$$

The overall dissipation is the sum of the surface and wake dissipations,

$$\Phi = \Phi_{\mathrm{surf}} + \Phi_{\mathrm{wake}} \tag{45}$$

$$\Phi_{\mathrm{surf}} = \int_0^{s_{\mathrm{TE}}} b\mathcal{D}\, \mathrm{d}s \tag{46}$$

$$\Phi_{\mathrm{wake}} = \int_{s_{\mathrm{TE}}}^{s_{\mathrm{end}}} b\mathcal{D}\, \mathrm{d}s \;+\; \Delta\Phi_{\mathrm{end}} \tag{47}$$

where $\Delta\Phi_{\mathrm{end}}$ is the additional dissipation of the wake portion which is downstream of the numerical wake end location s_{end}. This is estimated by approximate integration of the kinetic energy equation (12) from s_{end} to $s \to \infty$.

$$\begin{aligned} \Delta\Phi_{\mathrm{end}} = \int_{s_{\mathrm{end}}}^{\infty} b\mathcal{D}\, \mathrm{d}s &= \tfrac{1}{2}\rho_\infty V_\infty^3 \Theta^*_\infty \;-\; \left(\tfrac{1}{2}\rho_e u_e^3 \Theta^*\right)_{\mathrm{end}} \\ &+\; \frac{1}{2}\left[\, \rho_\infty V_\infty^2 \Delta^{**}_\infty + \left(\rho_e u_e^2 \Delta^{**}\right)_{\mathrm{end}} \right] \left[\, V_\infty - (u_e)_{\mathrm{end}} \right] \end{aligned} \tag{48}$$

The overall calculation gives reliable fuselage drag and dissipation predictions for any reasonable fuselage shape, without the need to rely on effective wetted area correlations, closure-angle correlations, or effective fineness-ratio correlations. For example, if the rear closure of the body is too rapid, the present method will predict separation off the back and into the wake, together with the increased dissipation leading to an increase in the downstream wake defect which reflects the larger drag.

4.5 Insensitivity to Perimeter Definition

It's useful to note that the individual 2D thicknesses θ, δ^* significantly depend on exactly how the effective perimeter b is defined. For example, in the wake where $b_0 = 0$, the momentum and kinetic energy area breakdowns become

$$\Theta = b\,\theta = 2\pi\delta^*\,\theta \tag{49}$$

$$\Theta^* = b\,\theta^* = 2\pi\delta^*\,\theta^* \tag{50}$$

So for example if the factor of 2π in the b definition (14) is modified somewhat because of a non-circular body cross section, then the θ, θ^* and δ^* values will change somewhat. However, because equations (11) and (12) evolve the full momentum and K.E. defects, these defects are extremely insensitive to how they are broken down into the θ, θ^*, and δ^* components in (49) and (50). So the computed drag and dissipation are also insensitive to such modeling ambiguities, since these depend only on the overall Θ, Θ^*, and $c_{\mathcal{D}}$. This justifies the somewhat ad-hoc definitions of b in the various integral area approximations.

For related reasons, the present drag and dissipation calculation method is surprisingly accurate for bodies which are not quite axisymmetric. If the flow is slender but not quite axisymmetric, the local 2D momentum defect $\rho_e u_e^2\,\theta$ might vary considerably at any given x location. In Figure 3, for example, the corresponding δ^* might be very nonuniform around the perimeter. A typical cause is redistribution of the viscous fluid via crossflow, from a small angle of attack, for instance. However, the circumferential integral of $\rho_e u_e^2 \theta$ will average out this redistribution, and since this integral is the total momentum defect,

$$\int \rho_e u_e^2\,\theta\;\mathrm{d}b = \rho_e u_e^2\,\Theta \tag{51}$$

the overall drag will also be very insensitive to such redistribution. The same argument follows for the kinetic energy thicknesses. Hence, accurate drag and dissipation predictions are still expected for weakly non-axisymmetric flows.

References

[1] T. Von Karman. Calculation of pressure distribution on airship hulls. Technical Memorandum 574, NACA, 1930.

[2] M. Drela. XFOIL: An analysis and design system for low Reynolds number airfoils. In T.J. Mueller, editor, *Low Reynolds Number Aerodynamics*. Springer-Verlag, Jun 1989. Lecture Notes in Engineering, No. 54, http://raphael.mit.edu/xfoil/.